INTERNATIONAL JOURNAL FOR NUMERICAL AND ANALYTICAL METHODS IN GEOMECHANICS
Int. J. Numer. Anal. Meth. Geomech. (2016)
Published online in Wiley Online Library (wileyonlinelibrary.com). DOI: 10.1002/nag.2633

Three dimensional elasto-plastic interface for embedded beam elements with interaction surface for the analysis of lateral loading of piles

Diego F. Turello[1,4], Federico Pinto[2,*,†] and Pablo J. Sánchez[3,4]

[1]*FCEFyN Universidad Nacional de Córdoba, CONICET, CP: 5000, Córdoba, Argentina*
[2]*FCEFyN Universidad Nacional de Córdoba, IDIT UNC-CONICET, Casilla de Correo 916, CP: 5000, Córdoba, Argentina*
[3]*CIMEC Universidad Nacional del Litoral-CONICET, Güemes 3450, CP: 3000, Santa Fe, Argentina*
[4]*GIMNI Universidad Tecnológica Nacional-FRSF, Lavaisse 610, CP: 3000, Santa Fe, Argentina*

SUMMARY

This paper presents a numerical formulation for a three dimensional elasto-plastic interface, which can be coupled with an embedded beam element in order to model its non-linear interaction with the surrounding solid medium. The formulation is herein implemented for lateral loading of piles but is able to represent soil-pile interaction phenomena in a general manner for different types of loading conditions or ground movements. The interface is formulated in order to capture localized material plasticity in the soil surrounding the pile within the range of small to moderate lateral displacements. The interface is formulated following two different approaches: (i) in terms of beam degrees of freedoms; and (ii) considering the displacement field of the solid domain. Each of these alternatives has its own advantages and shortcomings, which are discussed in this paper. The paper presents a comparison of the results obtained by means of the present formulation and by other well-established analysis methods and test results published in the literature. Copyright © 2016 John Wiley & Sons, Ltd.

Received 14 July 2016; Revised 7 September 2016; Accepted 14 September 2016

KEY WORDS: elasto-plastic interface; embedded beam elements; lateral loading; soil-pile interaction

1. INTRODUCTION

The analysis of lateral loading of piles can be performed by means of several techniques, such as: two dimensional beam over elastic foundation using the Winkler hypothesis [1–4], elastic analysis as proposed by Poulos [5] or Randolph [6], the $p - y$ method originally proposed by Reese *et al.* [7, 8], the Strain Wedge Method originally proposed by Norris *et al.* [9] and further developed by Ashour *et al.* [10, 11].

Although these approaches have been very useful in engineering practice, their application is not straightforward for the analysis of complex soil-structure interaction problems, where large pile groups, heterogeneous soils, and demands because of applied loads and ground movements are present. In these situations, an FE approach can provide some advantages, as it can readily account for several key features controlling the soil-structure interaction; for example, material elasto-plasticity, pile-soil-pile interaction in pile groups, installation effects, etc.

Sadek and Shahrour [12] proposed an Embedded Beam Element (EBE) formulation for the elastic analysis of piles in solid FE models, where the nodal pile displacements are written in terms of

*Correspondence to: Federico Pinto, FCEFyN Universidad Nacional de Córdoba - IDIT UNC-CONICET. Casilla de Correo 916, Córdoba, Argentina.
†E-mail: fpinto@unc.edu.ar

the nodal solid displacements through the interpolation of the solid (soil) elements. In this model, only the beam translational degrees of freedom (DOFs) are linked to solid DOFs, whereas the beam rotational DOFs remain as unknown variables of the problem. The main advantage of the classical EBE formulation is that it allows the interaction of two different kinds of finite elements (i.e., beams and solid), which are associated to different domains (i.e., pile and soil). Furthermore, the number of beam translational DOFs of the complete problem does not increase with the addition of embedded piles elements. Another key feature is that the beam mesh does not represent a constraint for the solid mesh generation, which can be adopted independently of the beam location. However, as a consequence of the fact that there is no explicit interaction surface between soil and pile, this formulation presents a mechanical incompatibility which produces non-convergent solutions when the pile nodes are close to or at the solid nodes. Engin *et al.* [13] show that the results obtained by means of the standard EBE for non-linear problems depend upon the mesh size of the model because of numerical instability and propose, as an ad-hoc solution, the definition of an elastic region around the pile axis where the behavior of the solid at the Gauss points is forced to remain elastic. These authors [14] and [15] have used this modified EBE formulation in order to estimate the behavior of pile groups.

Turello *et al.* [16] present an improved EBE formulation, which explicitly considers the interaction surface of the pile, where interaction forces –defined in terms of distributed forces– are accounted for within a well-posed mechanical framework.

As a novelty, this paper presents the formulation of an elasto-plastic interface, which is intended to represent the plasticity in the soil surrounding the pile, that can readily be coupled with the EBE formulation presented by Turello *et al.* [16]. Thus, the global pile-soil interaction problem is represented by means of the EBE formulation and the local plasticity in the soil next to the pile by means of the proposed interface. The interface is formulated so as to capture the initial states of plasticity in the solid domain (i.e., soil) and its effects on the structural response. An elasto-plastic constitutive law is considered in order to model the interaction forces in terms of the relative solid and beam displacements. The definition of the interface kinematics can be formulated in two different ways: (i) considering the displacement jump between solid and beam displacement fields along the beam axis, considering standard kinematic assumptions for the beam; and (ii) considering the relative displacements at the interaction surface by means of the full three dimensional (3D) solid kinematics.

The manuscript is organized as follows: Section 2 summarizes key aspects of the formulation of the previously proposed EBE with interaction surface [16]; Section 3 describes the proposed elasto-plastic interface within the EBE formulation; Section 4 discusses two alternative approaches for the definition of the constitutive laws for the proposed EBE model; Section 5 discusses the numerical performance of the proposed formulation showing comparisons against alternative approaches (such as: a $p-y$ method solution, strain wedge method, and field tests). The conclusions of this paper are summarized in Section 6.

Throughout the manuscript, the following nomenclature convention is adopted. Normal font is used to express mechanical objects based on 3D-solid kinematics, italic font means quantities based on technical beam-kinematics, whereas the hat-symbol over a variable implies nodal parameters. Lowercase and uppercase letters identify entities at the finite element level and global (assembled) level, respectively. Finally, double square brackets denote a displacement jump (i.e., a relative displacement).

2. OVERVIEW OF EMBEDDED BEAM ELEMENT FORMULATION WITH INTERACTION SURFACE

In this section, an overview of the EBE formulation, previously proposed by the authors, is presented. Full details of the formulation can be found in Turello *et al.* [16]. A sketch of the embedded beam element with explicit interaction surface is shown in Figure 1.

The main purpose of the EBE formulation proposed by Turello *et al.* is to explicitly represent the force interactions at the pile surface in order to avoid ill conditioning of the problem, which translates into singular stresses [16] and [13]. From a mechanical standpoint, this is naturally achieved

DOI: 10.1002/nag

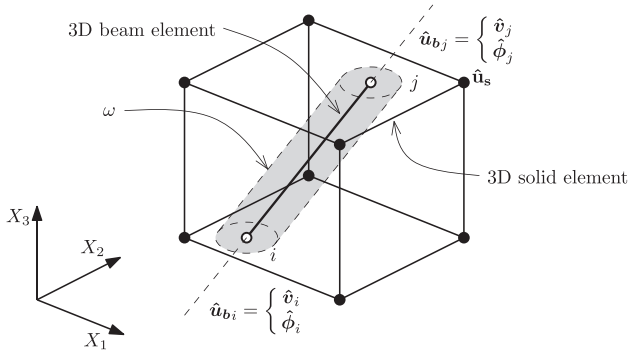

Figure 1. Layout of proposed Embedded Beam Element.

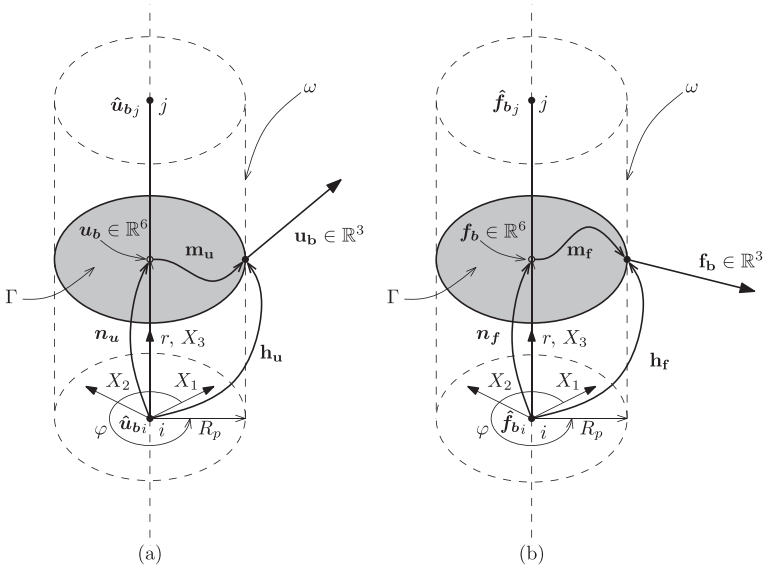

Figure 2. Layout of mapping operators: (a) $\mathbf{h_u}$ and (b) $\mathbf{h_f}$ in the proposed Embedded Beam Element with interaction surface ω.

by imposing a compatibility requirement between beam and solid displacements along the interaction surface. Full adherence between beam and solid is assumed for the elastic case. The system of interaction forces can be viewed as the system of reactive forces (r-forces) because of the kinematic restriction imposed at the interaction surface. In order to stress this important concept, and not to confuse it with another system of forces that will later be introduced in this paper also defined at the interaction surface, the interaction forces are referred to as *r-forces* in this paper.

As a starting point of this formulation, beam and solid displacements are defined by means of standard interpolation functions on the basis of nodal displacements (beam and solid) and rotations (beam only). Mapping functions are defined in order to express the beam displacements $\mathbf{u_b}$ and r-forces $\mathbf{f_b}$ (vectors in $\mathbb{R}^3$ at the interaction surface) as a function of the technical beam displacements $\boldsymbol{u_b}$ and r-forces $\boldsymbol{f_b}$ defined along the beam axis (vectors in $\mathbb{R}^6$), respectively (Figure 2).

2.1. Discretization and mapping functions

The 3D solid displacement vector field $\mathbf{u_s}$ is discretized by means of standard interpolation functions, $\mathbf{n_s}$, in terms of the spatial position, $\mathbf{X}$, and nodal parameters, $\hat{\mathbf{u}}_\mathbf{s}$:

$$\mathbf{u_s}(\mathbf{X}) = \mathbf{n_s}(\mathbf{X})\ \hat{\mathbf{u}}_\mathbf{s} \tag{1}$$

DOI: 10.1002/nag

The beam displacement vector field $\mathbf{u_b}$ at the interaction surface (Figure 2), is expressed as a function of the beam nodal displacements $\hat{\boldsymbol{u}}_{\boldsymbol{b}}$ (whose components are the displacements, $\hat{v}$, and the rotations, $\hat{\phi}$), by means of a mapping matrix $\mathbf{h_u}$, which is composed of the following: (i) an interpolation matrix $\boldsymbol{n_u}$ that defines the displacement field at the beam axis in terms of nodal displacements $\hat{\boldsymbol{u}}_{\boldsymbol{b}}$; and (ii) a mapping matrix $\mathbf{m_u}$ that converts displacements and rotations at the beam axis into a $\mathbb{R}^3$ vector displacement field at the interaction surface.

Figure 2 shows a layout of the interpolation and mapping operations, together with the global (X_1, X_2, X_3) and local (r, φ) coordinate systems for the case of a vertical pile with circular cross section (R_p is the radius of the pile). While the procedure can be generalized for other cross section geometries, this is not a straightforward task, as a new generalized mapping operator needs to be defined.

The interpolation matrix for beam displacements, $\boldsymbol{n_u}$, is defined in terms of the local position along the beam axis, r (Figure 2).

The mapping matrix $\mathbf{m_u}$ is defined in terms of the local cylindrical coordinate, φ, and takes into account the standard Navier–Bernoulli hypothesis, where the beam cross section Γ, remains planar, undeformed, and perpendicular to the beam axis. This hypothesis may be inaccurate for piles in stiff soils, where shear strains in the beam element may be significant because of the short characteristic length. However, the basis of the coupling formulation technique herein discussed remains valid if shear strains are accounted for, and will be implemented in future developments.

The vector field for beam displacements, $\mathbf{u_b}$, at the interaction surface can thus be written in terms of the beam nodal displacements, $\hat{\boldsymbol{u}}_{\boldsymbol{b}}$, as follows:

$$\mathbf{u_b}(r, \varphi) = \mathbf{h_u}(r, \varphi)\ \hat{\boldsymbol{u}}_{\boldsymbol{b}} = \mathbf{m_u}(\varphi)\ \boldsymbol{n_u}(r)\ \hat{\boldsymbol{u}}_{\boldsymbol{b}} \tag{2}$$

The explicit form of the mapping matrix, $\mathbf{h_u}$, for a 2-node (i.e., nodes i and j) cylindrical pile in local coordinates, as shown in Figure 2, is given in [16].

It is also assumed that the interaction r-force field, $\mathbf{f_b}$, at the interaction surface, can be expressed as a function of nodal beam interaction r-forces, $\hat{\boldsymbol{f}}_{\boldsymbol{b}}$, by means of the mapping matrix $\mathbf{h_f}$. The mapping scheme consists of two parts: (i) a matrix $\boldsymbol{n_f}$ that performs an interpolation of the beam r-forces $\boldsymbol{f_b}$, defined at the beam axis, in terms of nodal r-force values $\hat{\boldsymbol{f}}_{\boldsymbol{b}}$; and (ii) a mapping matrix $\mathbf{m_f}$ that converts the r-force system at the beam axis, $\boldsymbol{f_b}$, into a statically equivalent r-force system, $\mathbf{f_b}$, at the interaction surface. In other words, a specific structure for the reactive load system $\mathbf{f_b}$ is prescribed.

The interpolation matrix $\boldsymbol{n_f}$ is written in terms of the local coordinate r (Figure 2), whereas the matrix $\mathbf{m_f}$, that transfers the loads from the beam axis into the interaction surface, is defined in terms of the local coordinate φ.

The distributed r-force vector field $\mathbf{f_b}$, at the interaction surface, can thus be written as follows:

$$\mathbf{f_b}(r, \varphi) = \mathbf{h_f}(r, \varphi)\ \hat{\boldsymbol{f}}_{\boldsymbol{b}} = \mathbf{m_f}(\varphi)\ \boldsymbol{n_f}(r)\ \hat{\boldsymbol{f}}_{\boldsymbol{b}} \tag{3}$$

The explicit form of the mapping function $\mathbf{h_f}$ for a cylindrical pile is given in [16].

It should be noted that the interpolation matrices $\boldsymbol{n_u}$ and $\boldsymbol{n_f}$ are defined in terms of the r coordinate alone (Figure 2), whereas the mapping functions $\mathbf{h_u}$ and $\mathbf{h_f}$ are written in terms of local cylindrical coordinates r and φ. Another point to be emphasized is that the mapping operators $\mathbf{m_u}$ and $\mathbf{m_f}$ introduce modeling hypotheses (for kinematics and load distributions, respectively) at the continuum formulation level, irrespective of the numerical approximations adopted through $\boldsymbol{n_u}$ and $\boldsymbol{n_f}$.

2.2. Formulation of the Embedded Beam Element with interaction surface

As discussed in [16], the key feature of the EBE formulation with interaction surface is that it expresses the global stiffness matrix of the beam, $\boldsymbol{K_b}$, in terms of solid DOFs, $\mathbf{K_{bs}}$, and the stiffness matrix can readily be assembled to the solid stiffness matrix, in order to obtain the total stiffness matrix of the soil-pile system. Both, translational and rotational beam DOFs are transformed into equivalent solid DOFs.

DOI: 10.1002/nag

The problem is thus solved in terms of solid DOFs, whereas the beam DOFs can be subsequently obtained in a post-process step.

3. PROPOSED ELASTO-PLASTIC INTERFACE FORMULATION

In this section, an elasto-plastic interface between solid and beam elements is considered, in order to represent plastic strains in the soil within the vicinity of the pile[‡]. Thus, the hypothesis regarding perfect adherence of pile and soil is no longer enforced, and relative displacements because of plastic strains are introduced.

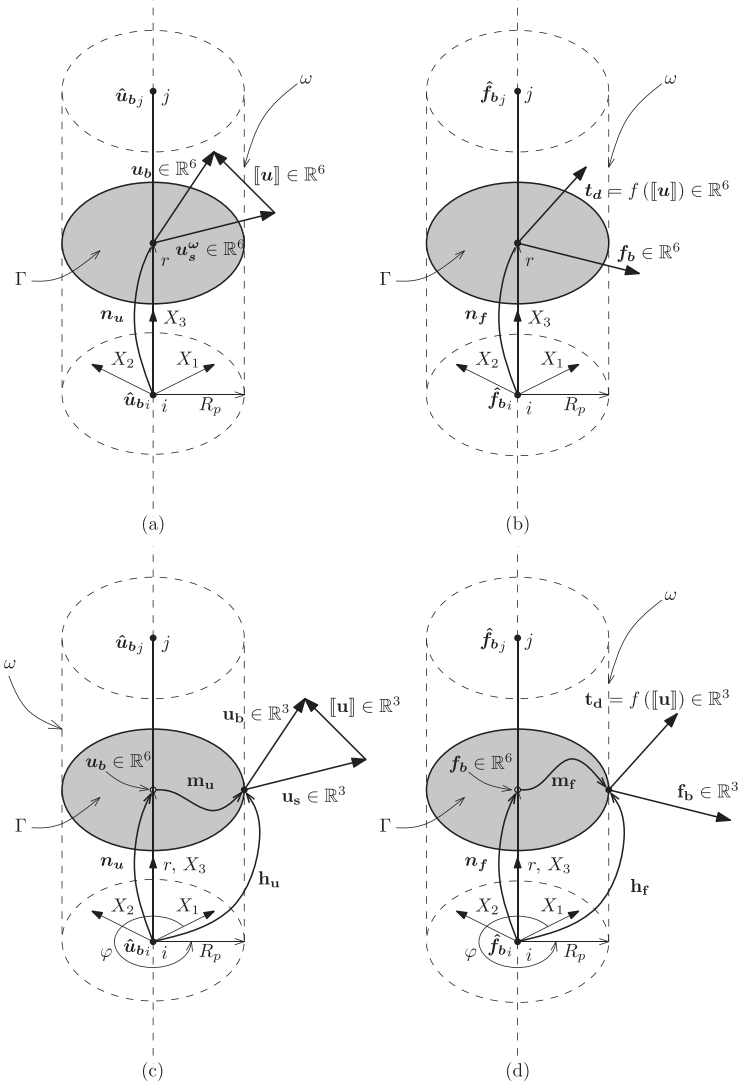

Figure 3. Layout of mechanical entities for embedded beam element with plastic interaction surface: (a) Displacements, and jumps, along the pile axis formulated on beam kinematics, (b) Interaction, r-forces and a-forces, along the pile axis, written using beam kinematics, (c) Mapping process showing displacements and jumps, at the interaction surface, expressed in terms of solids kinematics, (d) Mapping process displaying interactions force systems, r-force and a-force, at the interaction surface, written in terms of solids kinematics.

[‡]Eventually, generalized plasticity could be considered in the whole soil mass, through proper elasto-plastic constitutive laws in the 3D solid elements. However, this is not the aim of the present work.

DOI: 10.1002/nag

Therefore, a new (independent) kinematical descriptor is introduced into the mechanical formulation, $[\![\mathbf{u}]\!]$ (a vector in $\mathbb{R}^3$), whose physical meaning is the relative displacement between the beam and solid, as shown Figure 3-(c), associated to plastic strains developed in the near field and which is added to the elastic soil-structure response (obtained by means of the standard EBE formulation) in order to evaluate the total displacement of the pile. By using classical duality arguments, an additional system of interaction forces arises at the interaction surface, $\mathbf{t_d} \in \mathbb{R}^3$, for which a constitutive relation (in terms of $[\![\mathbf{u}]\!]$) is required (Figure 3-(d)). This additional system of forces is herein referred to a the *active-force system* (and will be denoted *a-force*), in order to differentiate it from the r-force system, $\mathbf{f_b} \in \mathbb{R}^3$, which is also introduced to guarantee a kinematical relation between beam and solid domains. Thus, it is important to keep in mind that, on the interaction surface, two force systems coexist: (i) the active forces ($\mathbf{t_d}$), defined by means of a constitutive model and non-linear in general; and (ii) the r-forces ($\mathbf{f_b}$), related to a kinematic compatibility requirement, as shown in Figure 3-(d). Both, $\mathbf{t_d}$ and $\mathbf{f_b}$, can also be expressed in terms of beam kinematics, $\boldsymbol{t_d}$ and $\boldsymbol{f_b}$, respectively, as shown in Figure 3-(b).

It is assumed that mapping functions, such as the ones given in Equation (2) and Equation (3), can also be applied to $[\![\mathbf{u}]\!]$ and $\mathbf{t_d}$, respectively. Thus, the following expressions can be written as follows:

$$[\![\mathbf{u}]\!] = \mathbf{h_u}\ [\![\hat{\boldsymbol{u}}]\!] = \mathbf{m_u}(\varphi)\ \boldsymbol{n_u}(r)\ [\![\hat{\boldsymbol{u}}]\!] \tag{4}$$

$$\mathbf{t_d} = \mathbf{m_f}(\varphi)\ \boldsymbol{t_d} \tag{5}$$

Because the EBE model couples two dissimilar kinematics (i.e., beam and solid), the relative displacements can be expressed in two alternative ways: either (i) in terms of beam kinematics, thus a constitutive model that links distributed interaction a-forces and moments versus relative displacements and rotations along the beam axis is warranted; or (ii) in terms of solid kinematics, for which a classical 3D constitutive model that links stresses versus strains on a thin zone representing the interaction surface needs to be introduced.

In the first case, for every pair of energy-conjugate variables (e.g., lateral a-force vs. lateral displacement) the constitutive law can be represented by means of a one dimensional (1D) model. In this context, the load-displacement methods, representing the non-linear soil response in lateral loading of piles (e.g., $p-y$ or $t-z$ methods), are widely accepted in the engineering practice and have been calibrated by several full scale load tests. Thus, definitions of this type of 1D constitutive relations, using the information of the $p-y$ (or $t-z$) methods, are adopted in this paper. Due to the fact that the $p-y$ (or $t-z$) curve represents the full elasto-plastic response of the piles, and that the elastic response in the proposed EBE approach is accounted for by the 3D FE model in the solid domain, the elastic contribution has to be subtracted from the $p-y$ curves in order to calibrate the interface. Thus, the full elasto-plastic response in the proposed modeling approach is represented by the interface (only plastic deformations) and the 3D FE model (elastic deformations). This mechanical model has to deal with the 3D nature of the problem by considering a 1D constitutive law that characterizes every couple of conjugate variables. Consequently, a projection scheme from the global reference axis onto the resultant bending plane is established, as the non-linearity of the problem precludes the consideration of two independent bending planes.

In the second case, an elasto-plastic constitutive model is formulated for the soil-pile domain representing the interaction region and is then projected onto the interaction surface, in order to obtain the required a-forces, $\mathbf{t_d}$, versus displacement jump, $[\![\mathbf{u}]\!]$, law. Following this approach, the 3D nature of the problem is naturally accounted for. Besides, as the relationship between stresses and strains is established by means of a general 3D solid constitutive model, additional effects could easily be incorporated into the problem by adopting well established 3D phenomenological models generally encountered in the soil mechanics field; for example, pore pressure generation and gapping.

These two alternative modelling approaches are discussed and compared in this paper.

DOI: 10.1002/nag

3.1. Formulation of the Embedded Beam Element with elasto-plastic interface

Compatibility of solid and beam displacements, including the existence of a relative displacement or jump $[\![\mathbf{u}]\!]$, is formulated at the entire interaction surface Ω ($\Omega = \cup_{e=1}^{e=Nb}\omega$, where ω stands for the interaction surface of each beam element, and N_b is the total number of beam elements).

A weak kinematic compatibility is enforced by imposing the condition that the relative displacement between the beam and solid plus the finite displacement jump, at the interaction surface, produces no virtual work with respect to any statically admissible system of virtual interaction r-forces, $\delta\mathbf{f_b}$ (this vector field at global level, and in terms of beam kinematics, is written as $\delta\boldsymbol{F}_{\boldsymbol{b}}$). Considering a standard FEM interpolation scheme, and using Equations (1), (2), (3), and (4), this restriction can be expressed as follows:

$$
\begin{aligned}
0 &= \mathop{\mathsf{A}}_{e=1}^{e=N_b} \int_{\omega} \delta\mathbf{f_b}^T \ (\mathbf{u_s} - \mathbf{u_b} + [\![\mathbf{u}]\!])\ \mathrm{d}\omega,\ \forall\ \delta\mathbf{f_b} \text{ statically admissible in the sense of Equation (3)} \\
0 &= \delta\hat{\boldsymbol{F}}_{\boldsymbol{b}}^T \left(\underbrace{\mathop{\mathsf{A}}_{e=1}^{e=N_b} \int_{\omega} \mathbf{h_f}^T\ \mathbf{n_s}\ \mathrm{d}\omega}_{\mathbf{A}^T}\ \hat{\mathbf{U}}_{\mathbf{s}} - \underbrace{\mathop{\mathsf{A}}_{e=1}^{e=N_b} \int_{\omega} \mathbf{h_f}^T\ \mathbf{h_u}\ \mathrm{d}\omega}_{\mathbf{B}^T}\ \left(\hat{\boldsymbol{U}}_{\boldsymbol{b}} - [\![\hat{\boldsymbol{U}}]\!]\right) \right),\ \forall\ \delta\hat{\boldsymbol{F}}_{\boldsymbol{b}} \\
0 &= \mathbf{A}^T\ \hat{\mathbf{U}}_{\mathbf{s}} - \mathbf{B}^T\ \left(\hat{\boldsymbol{U}}_{\boldsymbol{b}} - [\![\hat{\boldsymbol{U}}]\!]\right)
\end{aligned}
\tag{6}
$$

where $\hat{\mathbf{U}}_{\mathbf{s}}$ is the assembled vector of all solid nodal DOFs, $\hat{\boldsymbol{U}}_b$ is the assembled vector of all nodal beam DOFs, $[\![\hat{\boldsymbol{U}}]\!]$ is the assembled vector of all nodal displacement jumps DOFs, A is a FE assembly operator and the matrices $\mathbf{A}$ and $\mathbf{B}$ are defined as follows:

$$
\begin{aligned}
\mathbf{A} &= \mathop{\mathsf{A}}_{e=1}^{e=N_b} \int_{\omega} \mathbf{n_s}^T\ \mathbf{h_f}\ \mathrm{d}\omega \\
\mathbf{B} &= \mathop{\mathsf{A}}_{e=1}^{e=N_b} \int_{\omega} \mathbf{h_u}^T\ \mathbf{h_f}\ \mathrm{d}\omega
\end{aligned}
\tag{7}
$$

Note that the size of matrix $\mathbf{A}$ is given by the number of solid-DOFs times the number of beam-DOFs, whereas the size of matrix $\mathbf{B}$ is given by the number beam-DOFs squared. Thus, the assembly operator A must be properly constructed in each case.

It can be shown that if the same interpolation matrices for both, beam displacements $\boldsymbol{u_b}$ and interaction r-forces $\boldsymbol{f_b}$, are chosen (i.e., $\boldsymbol{n_u} = \boldsymbol{n_f}$), the matrix $\mathbf{B}$ yields invertible [16], which is a requirement in the present formulation. Another alternative is to adopt different discrete spaces for displacements and interaction r-forces, because the forces are usually interpolated by means of polynomials with lower degrees than the displacements. In this case, the regularity of matrix $\mathbf{B}$ is not automatically guaranteed and has to be checked in every case. In this paper, a beam element with linear interpolation for axial and torsional displacements and cubical interpolation for bending displacements is adopted, whereas the interaction r-forces are linearly interpolated. This combination gives an invertible $\mathbf{B}$ matrix. Thus, the nodal beam displacements could be expressed in terms of the nodal solid displacements and nodal displacement jumps as follows:

$$
\hat{\boldsymbol{U}}_{\boldsymbol{b}} = \mathbf{B}^{-T}\ \mathbf{A}^T\ \hat{\mathbf{U}}_{\mathbf{s}} + [\![\hat{\boldsymbol{U}}]\!] \tag{8}
$$

The next step is to relate the active with the r-force systems at the interaction interface. For this purpose, the balance of their corresponding virtual works under any admissible virtual displacement jump field of the entire pile, $\delta[\![\mathbf{u}]\!]$ is enforced. And then, by using Equations (3) and (4), the nodal interaction r-force vector, $\hat{\boldsymbol{F}}_{\mathbf{b}}$, can be written in terms of the distributed non-linear interaction

DOI: 10.1002/nag

a-forces along the beam axis, $\mathbf{t_d}$, as follows:

$$\begin{aligned}
&\mathop{\mathsf{A}}_{e=1}^{e=N_b} \int_\omega \delta[\![\mathbf{u}]\!]^T\ \mathbf{f_b}\ \mathrm{d}\omega = \mathop{\mathsf{A}}_{e=1}^{e=N_b} \int_\omega \delta[\![\mathbf{u}]\!]^T\ \mathbf{t_d}\ \mathrm{d}\omega,\ \forall\ \delta[\![\mathbf{u}]\!] \text{ kin. admissible in terms of Equation (4)} \\
&\delta[\![\hat{\boldsymbol{U}}]\!]^T \underbrace{\mathop{\mathsf{A}}_{e=1}^{e=N_b} \int_\omega \mathbf{h}_\mathbf{u}^T\ \mathbf{h_f}\ \mathrm{d}\omega}_{\mathbf{B}}\ \hat{\boldsymbol{F}}_{\boldsymbol{b}} = \delta[\![\hat{\boldsymbol{U}}]\!]^T \underbrace{\mathop{\mathsf{A}}_{e=1}^{e=N_b} \int_\omega \mathbf{h}_\mathbf{u}^T\ \mathbf{t_d}\ \mathrm{d}\omega}_{\hat{\boldsymbol{T}}_{\boldsymbol{d}}},\ \forall\ \delta[\![\hat{\boldsymbol{U}}]\!] \text{ kin. admissible} \\
&\mathbf{B}\ \hat{\boldsymbol{F}}_{\boldsymbol{b}} = \hat{\boldsymbol{T}}_{\boldsymbol{d}}
\end{aligned} \tag{9}$$

The non-linear global interaction a-force vector, $\hat{\boldsymbol{T}}_{\boldsymbol{d}}$, can be defined using solid kinematics as indicated in Equation (9), and rewritten for convenience here

$$\hat{\boldsymbol{T}}_{\boldsymbol{d}} = \mathop{\mathsf{A}}_{e=1}^{e=N_b} \int_\omega \mathbf{h}_\mathbf{u}^T\ \mathbf{t_d}\ \mathrm{d}\omega \tag{10}$$

where $\mathbf{t_d} \in \mathbb{R}^3$ is a 3D vector of interaction non-linear a-forces defined on each interaction surface ω (a constitutive relation for $\mathbf{t_d}$ needs to be prescribed).

As an alternative, the non-linear interaction a-force vector, $\hat{\boldsymbol{T}}_{\boldsymbol{d}}$, could be expressed in terms of beam kinematics. Replacing Equations (4) and (5) into Equation (10) yields:

$$\begin{aligned}
\hat{\boldsymbol{T}}_{\boldsymbol{d}} &= \mathop{\mathsf{A}}_{e=1}^{e=N_b} \int_\omega \boldsymbol{n}_{\boldsymbol{u}}^T\ \mathbf{m_u}^T\ \mathbf{m_f}\ \boldsymbol{t_d}\ \mathrm{d}\omega \\
\hat{\boldsymbol{T}}_{\boldsymbol{d}} &= \mathop{\mathsf{A}}_{e=1}^{e=N_b} \int_{l_p} \boldsymbol{n}_{\boldsymbol{u}}^T \left(\int_{\varphi=0}^{\varphi=2\pi} \mathbf{m}_\mathbf{u}^T\ \mathbf{m_f}\ R_p\ \mathrm{d}\varphi \right) \boldsymbol{t_d}\ \mathrm{d}l_p \\
\hat{\boldsymbol{T}}_{\boldsymbol{d}} &= \mathop{\mathsf{A}}_{e=1}^{e=N_b} \int_{l_p} \boldsymbol{n}_{\boldsymbol{u}}^T\ \boldsymbol{t_d}\ \mathrm{d}l_p
\end{aligned} \tag{11}$$

where l_p is the 1D-elemental beam domain (after assembling the elemental matrices this variable is written as L_p) and $\boldsymbol{t_d} \in \mathbb{R}^6$ is a vector that contains distributed interaction non-linear a-forces and moments along the beam axis (a constitutive model of the type $p - y$ or $t - z$, is required for $\boldsymbol{t_d}$).

From Equation (9), the nodal interaction r-force vector, $\hat{\boldsymbol{F}}_{\boldsymbol{b}}$, could be expressed in terms of the non-linear interaction a-force vector, $\hat{\boldsymbol{T}}_{\boldsymbol{d}}$, as follows

$$\hat{\boldsymbol{F}}_{\boldsymbol{b}} = \mathbf{B}^{-1}\ \hat{\boldsymbol{T}}_{\boldsymbol{d}} \tag{12}$$

By establishing the virtual work balance under a kinematically admissible virtual nodal displacement of the entire pile, $\delta\hat{\boldsymbol{U}}_{\boldsymbol{b}}$, and considering Equations (2) and (3), the equivalent load vector for the complete pile $\hat{\boldsymbol{P}}_{\boldsymbol{b}}$ (induced only by the system of interaction r-forces acting on the lateral pile surface), can be written in terms of $\hat{\boldsymbol{F}}_{\boldsymbol{b}}$ (and $\hat{\boldsymbol{T}}_{\boldsymbol{d}}$) as follows:

$$\begin{aligned}
&\delta\hat{\boldsymbol{U}}_{\boldsymbol{b}}^T\ \hat{\boldsymbol{P}}_{\boldsymbol{b}} = \delta\hat{\boldsymbol{U}}_{\boldsymbol{b}}^T \mathop{\mathsf{A}}_{e=1}^{e=N_b} \int_\omega \mathbf{h}_\mathbf{u}^T\ \mathbf{h_f}\ \mathrm{d}\omega\ \hat{\boldsymbol{F}}_{\boldsymbol{b}}, \quad \forall \quad \delta\hat{\boldsymbol{U}}_{\boldsymbol{b}} \text{ kinematically admissible} \\
&\hat{\boldsymbol{P}}_{\boldsymbol{b}} = \mathbf{B}\ \hat{\boldsymbol{F}}_{\boldsymbol{b}} = \hat{\boldsymbol{T}}_{\boldsymbol{d}}
\end{aligned} \tag{13}$$

The equivalent nodal load vector of the solid $\hat{\mathbf{P}}_\mathbf{s}$ (induced only by interactions forces), can be related to the system of r-forces, $\hat{\boldsymbol{F}}_{\boldsymbol{b}}$, by balancing their respective virtual works with respect to any kinematically admissible virtual displacement, $\delta\hat{\mathbf{U}}_\mathbf{s}$, of the solid nodes. Thus,

$$\begin{aligned}
&\delta\hat{\mathbf{U}}_\mathbf{s}^T\ \hat{\mathbf{P}}_\mathbf{s} = \delta\hat{\mathbf{U}}_\mathbf{s}^T \underbrace{\mathop{\mathsf{A}}_{e=1}^{e=N_b} \int_\omega \mathbf{n}_\mathbf{s}^T\ \mathbf{h_f}\ \mathrm{d}\omega}_{\mathbf{A}}\ \hat{\boldsymbol{F}}_{\boldsymbol{b}}, \qquad \forall \qquad \delta\hat{\mathbf{U}}_\mathbf{s} \text{ kinematically admissible} \\
&\hat{\mathbf{P}}_\mathbf{s} = \mathbf{A}\ \hat{\boldsymbol{F}}_{\boldsymbol{b}}
\end{aligned} \tag{14}$$

DOI: 10.1002/nag

Using Equation (12), $\hat{\mathbf{P}}_\mathbf{s}$ can be rewritten as a function of the non-linear interaction a-force vector, $\hat{\boldsymbol{T}}_{\boldsymbol{d}}$, as follows:

$$\hat{\mathbf{P}}_\mathbf{s} = \mathbf{A}\ \hat{\boldsymbol{F}}_{\boldsymbol{b}} = \mathbf{A}\ \mathbf{B}^{-1}\ \hat{\boldsymbol{T}}_{\boldsymbol{d}} \tag{15}$$

Finally, the complete system to be solved is composed by the discrete equilibrium equations of both domains, solid and beam, which can be rearranged as follows:

$$\begin{cases} -\mathbf{K}_\mathbf{s}\ \hat{\mathbf{U}}_\mathbf{s} + \hat{\mathbf{P}}_\mathbf{es} + \hat{\mathbf{P}}_\mathbf{s} & = \mathbf{0} \\ -\boldsymbol{K}_{\boldsymbol{b}}\ \hat{\boldsymbol{U}}_{\boldsymbol{b}} + \hat{\boldsymbol{P}}_{\boldsymbol{eb}} - \hat{\boldsymbol{P}}_{\boldsymbol{b}} & = \mathbf{0} \end{cases} \tag{16}$$

where $\hat{\mathbf{P}}_\mathbf{es}$ is the standard equivalent load vector because of external forces (e.g., surface tractions and body forces) applied to the solid, $\hat{\boldsymbol{P}}_{\boldsymbol{eb}}$ is the equivalent global load vector of the beam because of the lateral loads applied at the top of the pile, whereas $\mathbf{K}_\mathbf{s}$ and $\boldsymbol{K}_{\boldsymbol{b}}$ represent the standard (assembled) stiffness matrices for the solid and beam domains, respectively.

By considering Equations (13) and (15), the final system of equations yields as follows:

$$\begin{cases} -\mathbf{K}_\mathbf{s}\ \hat{\mathbf{U}}_\mathbf{s} + \hat{\mathbf{P}}_\mathbf{es} + \mathbf{A}\ \mathbf{B}^{-1}\ \hat{\boldsymbol{T}}_{\boldsymbol{d}} & = \mathbf{0} \\ -\boldsymbol{K}_{\boldsymbol{b}}\ \hat{\boldsymbol{U}}_{\boldsymbol{b}} + \hat{\boldsymbol{P}}_{\boldsymbol{eb}} - \hat{\boldsymbol{T}}_{\boldsymbol{d}} & = \mathbf{0} \end{cases} \tag{17}$$

where it becomes evident that the coupling is given through the interaction system of a-forces $\hat{\boldsymbol{T}}_{\boldsymbol{d}}$.

The system of Equations (17) is subject to classical kinematical boundary conditions on the Dirichlet boundary of the solid and the constraint imposed by the displacements compatibility, given in Equation (8), which can be re-written as follows:

$$[\![\hat{\boldsymbol{U}}]\!] = \hat{\boldsymbol{U}}_{\boldsymbol{b}} - \mathbf{B}^{-T}\ \mathbf{A}^{T}\ \hat{\mathbf{U}}_\mathbf{s} \tag{18}$$

4. INTERFACE CONSTITUTIVE MODELS

4.1. Constitutive model for $\boldsymbol{t}_{\boldsymbol{d}}$ based on beam kinematics

In this case, the input variable for the constitutive model is the displacement jump along the beam axis, $[\![\boldsymbol{u}]\!]$, defined in terms of the beam kinematics. The constitutive model yields the non-linear interaction a-forces defined also in terms of beam kinematics; that is, distributed loads and moments along the beam axis, $\boldsymbol{t}_{\boldsymbol{d}}$.

The displacement jump $[\![\boldsymbol{u}]\!]$ on a point with local coordinates along the beam axis r (Figure 3-(a)), is written as follows:

$$[\![\boldsymbol{u}]\!] = \boldsymbol{u}_{\boldsymbol{b}} - \boldsymbol{u}_{\boldsymbol{s}}^{\boldsymbol{\omega}} \tag{19}$$

where $\boldsymbol{u}_{\boldsymbol{s}}^{\boldsymbol{\omega}}$ is the solid displacement field evaluated over the interaction surface ω and mapped onto the beam axis by means of the kinematics assumed for the beam domain. The global counterpart of Equation (19) is given by Equation (18).

The displacement jump over the beam axis, $[\![\boldsymbol{u}]\!]$, is characterized by means of six components (three displacement jumps and three rotation jumps). Nevertheless, the constitutive model is defined in terms of only four components as it is shown in Figure 4, due to the fact that the mechanical response cannot be considered independently along Cartesian components when plastic strains are allowed in the soil. In Figure 4, the π-axis, aligned with the resultant lateral displacement jump vector $[\![v_\pi]\!]$, and the ζ-axis (being orthogonal to π-axis) aligned with the resultant rotation jump vector $[\![\phi_\zeta]\!]$, both associated with bending, are displayed on a point with local coordinates along the beam axis r. Hence, the jump components are the following: the lateral displacement jump along the π-axis $[\![v_\pi]\!]$, the axial displacement jump $[\![v_3]\!]$, the rotation jump along the ζ-axis $[\![\phi_\zeta]\!]$, and the torsional rotation jump along the beam axis $[\![\phi_3]\!]$. These components are grouped together into an equivalent displacement jump vector $[\![\boldsymbol{u}^*]\!] \in \mathbb{R}^4$. This equivalent reduced displacement vector is

DOI: 10.1002/nag

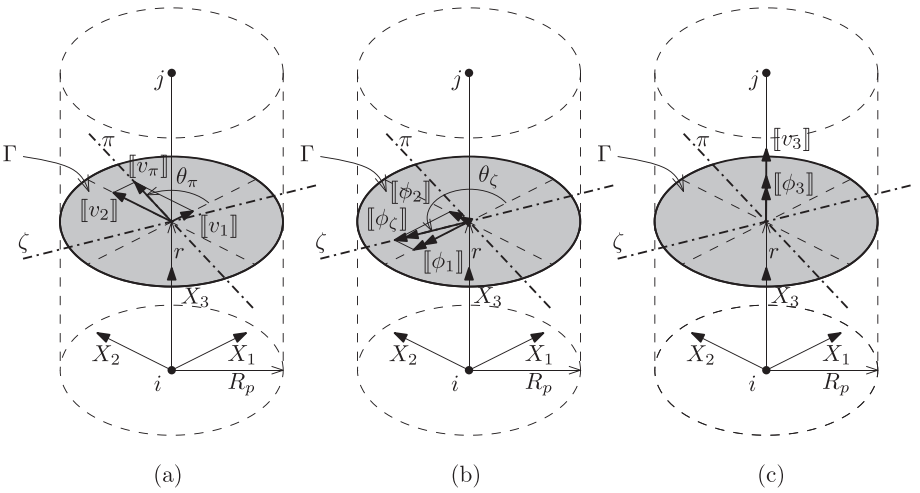

Figure 4. Components of the displacement vector jump $[\![\boldsymbol{u}^*]\!]$: (a) displacement component along π-axis $[\![v_\pi]\!]$ (b) rotation component along ζ-axis $[\![\phi_\zeta]\!]$ and (c) components along the beam axis $[\![v_3]\!]$ and $[\![\phi_3]\!]$.

written in terms of the six components of displacement jumps using the projection operator $\mathcal{P}$ as the following:

$$
\begin{aligned}
[\![\boldsymbol{u}^*]\!] &= \mathcal{P}\,[\![\boldsymbol{u}]\!] \\
\begin{pmatrix} [\![v_\pi]\!] \\ [\![v_3]\!] \\ [\![\phi_\zeta]\!] \\ [\![\phi_3]\!] \end{pmatrix} &= \begin{pmatrix} \cos\theta_\pi & \sin\theta_\pi & 0 & 0 & 0 & 0 \\ 0 & 0 & 1 & 0 & 0 & 0 \\ 0 & 0 & 0 & \cos\theta_\zeta & \sin\theta_\zeta & 0 \\ 0 & 0 & 0 & 0 & 0 & 1 \end{pmatrix} \begin{pmatrix} [\![v_1]\!] \\ [\![v_2]\!] \\ [\![v_3]\!] \\ [\![\phi_1]\!] \\ [\![\phi_2]\!] \\ [\![\phi_3]\!] \end{pmatrix}
\end{aligned} \tag{20}
$$

where θ_π and θ_ζ are the angles between the global axis X_1 and the resultant lateral jump along π-axis and the resultant rotation jump along ζ-axis, respectively, as it is shown in Figure 4.

The equivalent non-linear reduced interaction a-force vector, $\boldsymbol{t}_{\boldsymbol{d}}^* \in \mathbb{R}^4$, is defined in terms of the equivalent displacement jump vector $[\![\boldsymbol{u}^*]\!] \in \mathbb{R}^4$ as follows:

$$
\boldsymbol{t}_{\boldsymbol{d}}^* = f\left([\![\boldsymbol{u}^*]\!]\right) \tag{21}
$$

The constitutive model, $\boldsymbol{t}_{\boldsymbol{d}}^* = f\left([\![\boldsymbol{u}^*]\!]\right)$, relates each component of the displacement jump vector (defined along the beam axis) with the corresponding distributed interaction a-force. Thus, the following conjugate pairs are defined: the lateral displacement jump, $[\![v_\pi]\!]$, versus the lateral distributed interaction a-force, t_π, along the π-axis; the axial displacement jump, $[\![v_3]\!]$, versus the axial distributed interaction a-force, t_3; the rotation jump associated with bending, $[\![\phi_\zeta]\!]$, versus the distributed bending a-moment, m_ζ, along the ζ-axis; and the torsional rotation jump along the beam axis, $[\![\phi_3]\!]$, versus the distributed torsional a-moment, m_3.

In this paper, two kinds of 1D elasto-plastic models are adopted for each conjugated pairs (see more details in [17]), namely: (i) a bi-linear model with linear hardening and with limit load for granular soils; and (ii) a model with exponential hardening for cohesive materials.

A sketch of the proposed models is given in Figure 5, where the typical curves for t_π versus $[\![v_\pi]\!]$ are shown. The curves for the other components are constructed in a similar way. In this figure, $C_{t\pi}^{ep}$ is the elasto-plastic tangent modulus, and $C_{t\pi}^{e}$ is the initial elastic interface stiffness. As the global elastic response of the soil mass is taken into account by the full 3D FE model of the soil, the elastic strain component at the interface needs to be minimized. This is attained by defining a fictitiously large elastic stiffness at the interface. In order to obtain the initial elastic interface stiffness for the different types of loadings, a simple methodology (Figure 6) is proposed, where the initial elastic interface stiffness is estimated as the elastic stiffness of a ring surrounding the pile with an elastic

DOI: 10.1002/nag

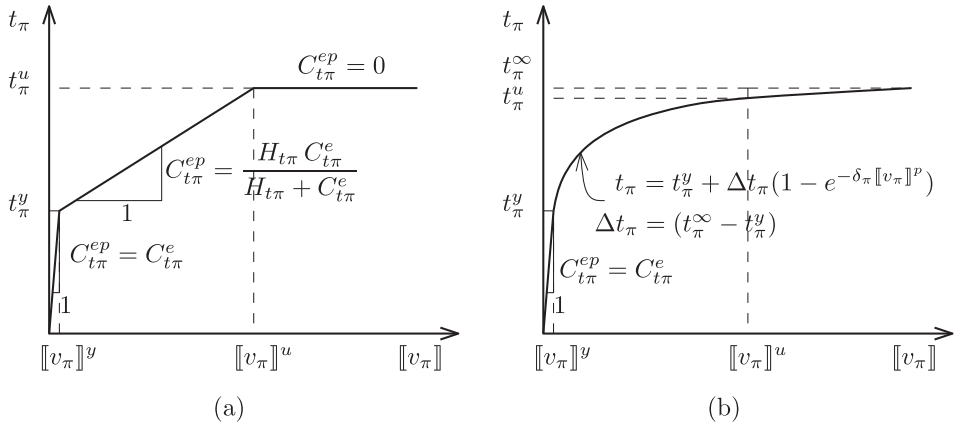

Figure 5. One dimensional elasto-plastic model to characterize t_π versus $[\![v_\pi]\!]$: (a) bi-linear model with linear hardening and (b) exponential hardening.

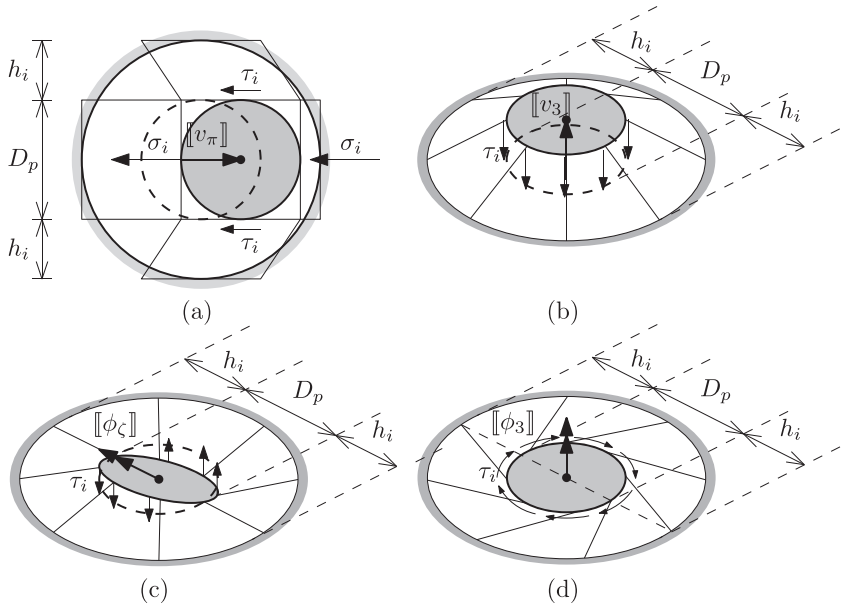

Figure 6. Sketch of the ring-model used to estimate the initial elastic interface stiffness of the pile for different loading modes: (a) lateral stiffness $C^e_{t\pi}$ (b) axial stiffness C^e_{t3} (c) flexural stiffness $C^e_{m\zeta}$ and (d) torsional stiffness C^e_{m3}. In this methodology, σ_i and τ_i are the normal and shear stresses at the pile-ring interface.

shear modulus G_i, Poisson coefficient ν_i and fictitious thickness h_i[§]. In this paper, an elastic shear modulus for the ring $G_i = 2\,\text{to}\,5\ G_s$ is adopted, where G_s is the elastic shear modulus of the soil, whereas the Poisson ratio $\nu_i = \nu_s$ and $h_i = 0.10 D_p$. The adopted expressions for the initial stiffness coefficients, according to different loading modes, are shown in Table I.

Due to the fact that the $p - y$ method is widely used in the engineering practice, the proposed 1D elasto-plastic models are calibrated in order to fit key parameters of the $p - y$ curves; for example, the ultimate load, the yield load and the ultimate relative displacement. Moreover, the non-linear interface parameters of the present approach are expressed in terms of the solid parameters and the ones used in the $p - y$ curve definition. In what follows, the procedure to characterize the a-force along π-axis for the lateral displacement case t_π is described as follows:

[§]In this work, h_i is adopted as a fraction of the pile diameter D_p

DOI: 10.1002/nag

Table I. Initial elastic interface stiffness for different loading modes given in Figure 6.

Initial elastic stiffness	
$C^e_{t\pi}$	$\frac{G_i}{h_i}\ 2\ (3+2\nu_i)$
C^e_{t3}	$\frac{G_i\,\pi}{h_i}$
$C^e_{m\zeta}$	$\frac{G_i\,\pi\,D_p^2}{8\,h_i}$
C^e_{m3}	$\frac{G_i\,\pi\,D_p^2}{4\,h_i}$

(i) The ultimate load in the bi-linear model, t^u_π (being the ultimate load of the 1D plasticity model depicted in Figure 5-(a)), is adopted as the ultimate load from the $p-y$ curve, whereas in the exponential model, t^∞_π (Figure 5-(b)), is adopted as the ultimate load for very large lateral displacements and $t^u_\pi = 98\%\ t^\infty_\pi$.

(ii) The lateral yield load is adopted as $t^y_\pi = a_y\ t^u_\pi$, where a_y is an internal parameter which is adopted in order to fit the yielding loads in the corresponding $p-y$ curves.

(iii) The ultimate displacement jump $[\![v_\pi]\!]^u$, in the proposed 1D elasto-plastic model (Figure 5), is defined by subtracting the elastic displacement component from the ultimate displacements in the $p-y$ curve, which is estimated as $\frac{t^u_\pi}{k_s}$, k_s being the soil-pile lateral reaction modulus estimated from Vesic [18]. The displacement jump at yielding, $[\![v_\pi]\!]^y$, is estimated from the definition of the lateral yield load and the correspondent initial elastic interface stiffness given by: $[\![v_\pi]\!]^y = \frac{t^y_\pi}{C_{t\pi}}$.

(iv) In the bi-linear model, the linear hardening plastic modulus, $H_{t\pi}$ (Figure 5-(a)), is defined in order to fit the $p-y$ curve, and takes the form as follows:

$$H_{t\pi} = \frac{C^e_{t\pi}\left(t^u_\pi - t^y_\pi\right)}{C^e_{t\pi}[\![v_\pi]\!]^u - t^u_\pi} \tag{22}$$

(v) Finally, δ_π is a model parameter that characterizes the exponential hardening (Figure 5-(b)) also defined in order to fit the $p-y$ curve[¶], and $[\![v_\pi]\!]^p$ is the cumulative equivalent plastic displacement at the interface. The parameter δ_π is defined as follows:

$$\delta_\pi = -\ln\left(\frac{t^\infty_\pi - t^y_\pi}{t^\infty_\pi - t^u_\pi}\right)\frac{C^e_{t\pi}}{C^e_{t\pi}[\![v_\pi]\!]^u - t^u_\pi} \tag{23}$$

The curves for other types of loadings conditions can be described in a similar way using the $p-y$ or $t-z$ method. In this work, considering that single vertical piles carrying large torsional loads are rarely encountered in practice, the curves corresponding to the torsional load are adopted as fully elastic. Nevertheless, a 1D elasto-plastic model can easily be defined by following the procedure described previously.

A comparison of the proposed 1D constitutive model for lateral behavior and the $p-y$ curves proposed by Reese *et al.* [7, 8] is shown in Figure 7 for both sand and clay, for a depth of $z = 15.00$ m. The pile diameter is $D_p = 0.50$ m, whereas the soil parameters adopted for the sand (and for the definition of the $p-y$ curve) are as follows: Young's modulus $E_s = 216$ MPa, Poisson coefficient $\nu_s = 0.25$, unit soil weight $\gamma_s = 16\,\mathrm{kN/m^3}$, internal friction angle $\phi_s = 32°$, increment of soil reaction modulus with depth $m_h = 40\,\mathrm{MPa/m}$. The fictitious thickness of the interface is $h_i = 0.10 D_p$, and the internal parameter a_y is adopted as $a_y = 0.20$. The clay model, in terms of total stresses, considers an undrained shear strength $s_u = 0.01$ MPa, unit soil weight $\gamma_s =$

[¶]The model parameter δ_π is defined with proper units in order to give a dimensionless exponent in Figure 5-(b). In this case, for the lateral displacements, the units are L^{-1}.

DOI: 10.1002/nag

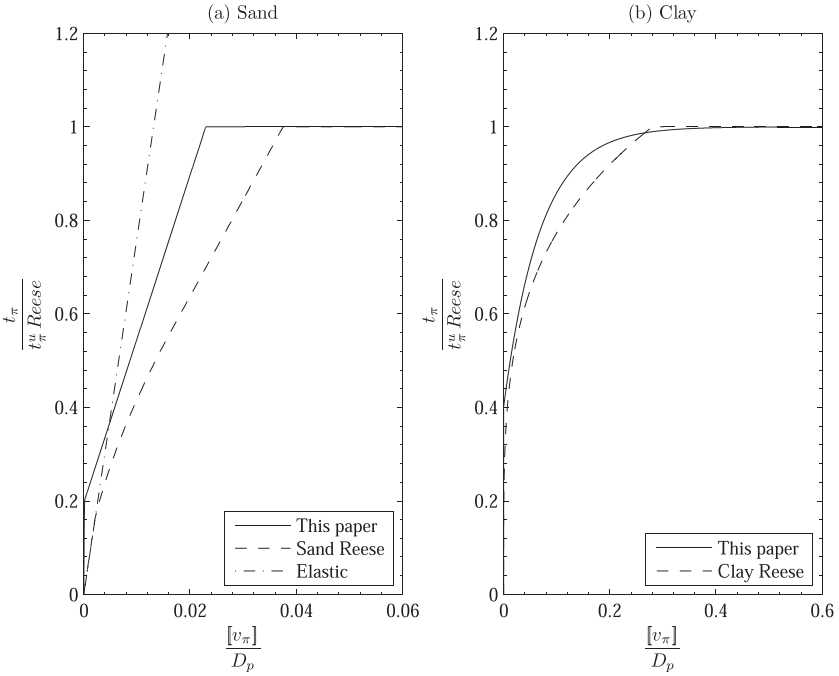

Figure 7. Proposed elasto-plastic one dimensional model and $p-y$ curves for $z = 15.00\,\mathrm{m}$ in the t_π versus $[\![v_\pi]\!]$ component for: (a) bi-linear model with linear hardening and (b) exponential hardening.

$16\,\mathrm{kN/m^3}$, increment of soil reaction modulus with depth $m_h = 20\,\mathrm{MPa/m}$. In this case, the internal parameter is $a_y = 0.40$.

It can be seen from Figure 7 that the proposed 1D elasto-plastic model fits the ultimate and yield loads obtained by means of the $p-y$ curves, whereas the general response is stiffer due to the fact that the lateral displacement jump in the proposed approach neglects the initial elastic displacement component present in the $p-y$ curves.

The energy-conjugate couples in Equation (21) are assumed to be independent from each other; hence, the derivative of the distributed interaction forces $\boldsymbol{t}_{\boldsymbol{d}}^{*}$ with respect to $[\![\boldsymbol{u}^{*}]\!]$ can be written as follows:

$$\boldsymbol{C_d} = \frac{\partial \boldsymbol{t}_{\boldsymbol{d}}^{*}}{\partial [\![\boldsymbol{u}^{*}]\!]} = \begin{pmatrix} C_{t\pi}^{ep} & 0 & 0 & 0 \\ 0 & C_{t3}^{ep} & 0 & 0 \\ 0 & 0 & C_{m\zeta}^{ep} & 0 \\ 0 & 0 & 0 & C_{m3}^{ep} \end{pmatrix} \tag{24}$$

where $\boldsymbol{C_d}$ is the interface tangent modulus matrix (Figure 5).

Next, the components of the interaction a-force vector $\boldsymbol{t_d} \in \mathbb{R}^6$ are obtained by transforming the equivalent interaction a-force $\boldsymbol{t}_{\boldsymbol{d}}^{*}$ over the pile axis in the coordinate system X_1, X_2, X_3

$$\begin{gathered} \boldsymbol{t_d} = \mathcal{P}^T \boldsymbol{t}_{\boldsymbol{d}}^{*} \\ \begin{pmatrix} t_1 \\ t_2 \\ t_3 \\ m_1 \\ m_2 \\ m_3 \end{pmatrix} = \begin{pmatrix} \cos\theta_\pi & 0 & 0 & 0 \\ \sin\theta_\pi & 0 & 0 & 0 \\ 0 & 1 & 0 & 0 \\ 0 & 0 & \cos\theta_\zeta & 0 \\ 0 & 0 & \sin\theta_\zeta & 0 \\ 0 & 0 & 0 & 1 \end{pmatrix} \begin{pmatrix} t_\pi \\ t_3 \\ m_\zeta \\ m_3 \end{pmatrix} \end{gathered} \tag{25}$$

DOI: 10.1002/nag

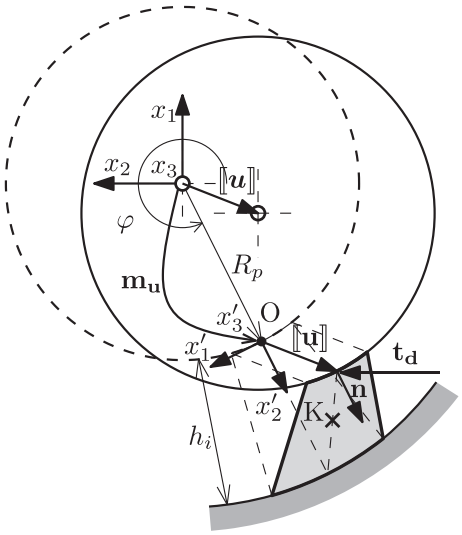

Figure 8. Sketch of the interface expressed in solid kinematics. Transverse section view. Displacement jump $[\![\mathbf{u}]\!]$ at the point O for the evaluation of stresses at the point K in the ring, which projected over the normal vector $\mathbf{n}$ gives the interaction a-forces $\mathbf{t_d}$. The vectors x_3 and x'_3 are out-of-plane vectors, normal to the figure.

4.2. Constitutive model for $\mathbf{t_d}$ *based on solid kinematics*

In this section, the constitutive model is formulated in terms of a conventional 3D stress-strain law in a narrow domain around the pile, representing the interaction surface, ω. Figure 3-(c) and 3-(d) show the kinematic variables and the interaction a-forces, respectively, considered in order to describe the non-linear interface. It should be noted that, in the present approach, additional hypotheses regarding projection schemes are not warranted, because the mechanical formulation naturally captures the three-dimensionality of the problem.

In this case, the non-linear interaction a-forces, $\mathbf{t_d} \in \mathbb{R}^3$, are defined in terms of the displacement jump, $[\![\mathbf{u}]\!] \in \mathbb{R}^3$, as shown in Figure 3-(c) and 3-(d). The displacement jump is assumed to develop between the interaction surface and a fictitious surface (at an offset, h_i, from the interaction surface ω, as shown in Figure 8). By doing so, a soil ring surrounding the pile is defined, which is modeled by means of a fully 3D elasto-plastic constitutive law. Thus, h_i becomes a new parameter of this model, which has to be characterized according to the thickness where localized plastic strains are taking place.

Figure 8 shows a generic transverse section of a circular pile together with the local Cartesian coordinate system, $x_1,\ x_2,\ x_3$ (x_3 is an out-of-plane vector, normal to the figure). This figure also shows the point O, on the interaction surface, defined by means of a cylindrical coordinate system $\varphi,\ R_p$. Another local Cartesian coordinate system, $x'_1,\ x'_2,\ x'_3$, is used in order to define the normal and tangential components of the displacement jump $[\![\mathbf{u}]\!]$. In this case, the vector normal to the interaction surface, $\mathbf{n}$, is coincident with the axis x'_2. The transformation between the coordinate systems $(x_1,\ x_2,\ x_3)$ and $\left(x'_1,\ x'_2,\ x'_3\right)$ is performed by means of a conventional rotation matrix $\mathbf{Q}$, defined as follows:

$$\mathbf{Q} = \begin{pmatrix} -\cos\varphi & \sin\varphi & 0 \\ -\sin\varphi & -\cos\varphi & 0 \\ 0 & 0 & 1 \end{pmatrix} \tag{26}$$

where φ is defined in Figure 8.

The displacement jump on the interaction surface, $[\![\mathbf{u}]\!]$, is first written by means of Equation (4) and then expressed in terms of the local coordinate system, $[\![\mathbf{u}']\!]$, through the rotation matrix $\mathbf{Q}$, as follows:

$$[\![\mathbf{u}']\!] = \mathbf{Q}\,[\![\mathbf{u}]\!] \tag{27}$$

DOI: 10.1002/nag

In this paper, it is assumed that the deformation gradient is constant through the fictitious thickness h_i and along the n-direction. The strain tensor in the soil interface, $\boldsymbol{\varepsilon_i}$, because of the displacement jump $[\![\mathbf{u}']\!]$ at a point K (Figure 8), can be written as follows:

$$\boldsymbol{\varepsilon_i} = \frac{[\![\mathbf{u}']\!] \otimes^s \mathbf{n}}{h_i} \tag{28}$$

where $\otimes^s$ represents the symmetric tensor product.

The stress tensor at the interface, $\boldsymbol{\sigma_i}$, is obtained as the sum of a previous stress state, $\boldsymbol{\sigma_i^p}$, plus a stress increment, $\Delta\boldsymbol{\sigma_i}$, which is related to the strain tensor increment, $\Delta\boldsymbol{\varepsilon_i}$, by means of a 3D constitutive model. Thus, $\boldsymbol{\sigma_i}$ is written as follows:

$$\boldsymbol{\sigma_i} = \boldsymbol{\sigma_i^p} + \Delta\boldsymbol{\sigma_i} = \boldsymbol{\sigma_i^p} + \boldsymbol{C^{ep}} : \Delta\boldsymbol{\varepsilon_i} \tag{29}$$

where $\boldsymbol{C^{ep}}$ is the fourth-order tangent elasto-plastic constitutive tensor. In this work, two different 3D laws are implemented: (i) a Modified Cam Clay (MCC), as described in [19], for materials that undergo plastic strains under hydrostatic and deviatoric strains states; and (ii) a J2 plasticity model with a limit pressure and tension cut-off for modeling undrained behavior of saturated clays in total stresses. Linear hardening and associated plasticity are adopted for both models.

Before the deformation process because of external loadings, the previous stress state, $\boldsymbol{\sigma_i^p}$, coincides with a predefined initial stress state $\boldsymbol{\sigma_i^0}$. For simplicity, in this paper, the initial stress state, $\boldsymbol{\sigma_i^0}$, is considered as an isotropic stress state. However, the effects of deviatoric components in the initial stress field can readily be accounted for (e.g., by means of a K_o stress state ratio between vertical and horizontal components).

The non-linear interaction a-forces, $\mathbf{t'_d}$, at the point O on the interaction surface expressed in the local coordinate system (x_1', x_2', x_3'), are obtained by projecting the stress state at the point K, as follows:

$$\mathbf{t'_d} = \boldsymbol{\sigma_i} \cdot \mathbf{n} \tag{30}$$

Finally, the non-linear interaction a-forces at point O, $\mathbf{t_d} \in \mathbb{R}^3$, written in the local Cartesian coordinate system (x_1, x_2, x_3) are obtained by rotating the components of $\mathbf{t'_d}$ through the matrix $\mathbf{Q}$, as follows:

$$\mathbf{t_d} = \mathbf{Q}^T \mathbf{t'_d} \tag{31}$$

5. VALIDATION

5.1. Preliminaries

In this paper, the EBE formulation is implemented for two types of solid elements: an 8-node bi-linear brick element with reduced-integration (referred to as H8) and a 27-node bi-quadratic brick element (referred to as H27). The interpolation functions for both elements belong to the $\mathcal{C}^0$ space [20].

For the beam domain a 2-node beam element is considered, referred to as B2, with standard Hermite cubic interpolation functions for lateral displacements (interpolation functions belong to the $\mathcal{C}^1$ space) and standard linear interpolation functions for axial and torsional displacements (interpolation functions belong to the $\mathcal{C}^0$ space).

The interface model defined in terms of beam kinematics, and characterized by means of 1D models that represent standard $p - y$ curves, is referred to as PY, whereas the interface model described in terms of solid kinematics, and considering a fully 3D MCC constitutive model, is referred to as CC.

Combining the solid and beam elements described previously, and considering the different interfaces, the embedded beam elements H8B2-PY, H27B2-PY, H8B2-CC, and H27B2-CC are derived. The *Elastic* reference solution is used to denote the response obtained by means of the H8B2 EBE assuming perfect adherence between pile and soil following the EBE formulation proposed by the authors [16].

DOI: 10.1002/nag

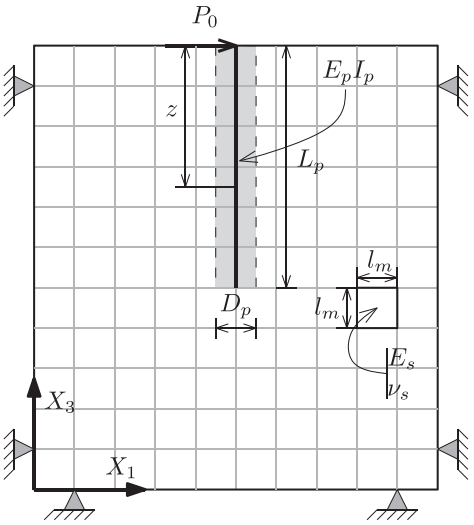

Figure 9. Pile in a cohesionless soil. Lateral view of the three dimensional example.

5.2. Pile in a cohesionless soil

In this section, the key features of the proposed EBE formulation with elasto-plastic interface are assessed for a vertical pile under lateral loading in a cohesionless Gibson soil (i.e., linear increase of stiffness with depth). A lateral view of this 3D problem is shown in Figure 9, where the geometry, the external loads and boundary conditions are illustrated. The numerical results obtained by means of the proposed formulation are compared with: (i) the results obtained by means of the $p-y$ method, considering in this case the curve for sand proposed by Reese *et. al.* [21]; and (ii) the elastic solution obtained by means of the EBE formulation with explicit interaction surface previously proposed by the authors [16] (i.e., assuming perfect adherence between pile and soil).

The soil parameters (used for modeling the solid domain) are as follows: Young's modulus $E_s = 14.42\,\mathrm{MN/m^3} \times z$, Poisson coefficient $\nu_s = 0.25$, soil unit weight $\gamma_s = 16\,\mathrm{kN/m^3}$, and internal friction angle $\phi_s = 32°$.

The proposed non-linear interface, described in terms of beam kinematics, uses 1D-plasticity models with bi-linear hardening as shown in Figure 5-(a), for each component of $\mathbf{t'_d}$. These curves are characterized by the rate of increase of reaction modulus with depth, $m_h = 60\,\mathrm{MPa/m}$, as well as the remaining soil and beam parameters defined previously. The fictitious thickness of the interface is $h_i = 0.10 D_p$, and the internal parameter a_y is adopted as $a_y = 0.20$.

The proposed interface described in terms of solid kinematics considers the 3D elasto-plastic MCC model (full details are given [19]), which are as follows: internal material constant $\beta = 0.70$, tensile yield hydrostatic stress $p_t \approx 0\,\mathrm{MPa}$, compressive yield hydrostatic stress $p_c = -\gamma_s\, z$, critical state line slope $M_c = \frac{6\sin(\phi_s)}{3-\sin(\phi_s)} = 1.287$, and linear hardening modulus $H = 0.20$.

The beam domain is characterized by the pile properties, namely: Young's modulus $E_p = 30{,}000\,\mathrm{MPa}$, length $L_p = 15.00\,\mathrm{m}$, diameter $D_p = 0.50\,\mathrm{m}$, and second moment of area $I_p = \frac{\pi D_p^4}{64}$.

Figure 10-(a) shows the normalized lateral displacements along the pile in terms of the normalized depth, where a good agreement is observed between the $p-y$ method and the numerical solution obtained by means of the proposed formulation, both for the interface model expressed in terms of beam and solid kinematics.

Figure 10-(b) and 10-(c) displays the normalized internal forces (bending moments and shear forces, respectively) in terms of the normalized depth, where it can be seen that the results obtained by means of the proposed formulation are in good agreement with those obtained by the $p-y$ method. In this case, H8B2-CC and H27B2-CC EBEs yield internal forces larger than those obtained by the H8B2-PY and H27B2-PY EBEs.

Table II depicts key numerical results and their relative position for different EBEs and different

DOI: 10.1002/nag

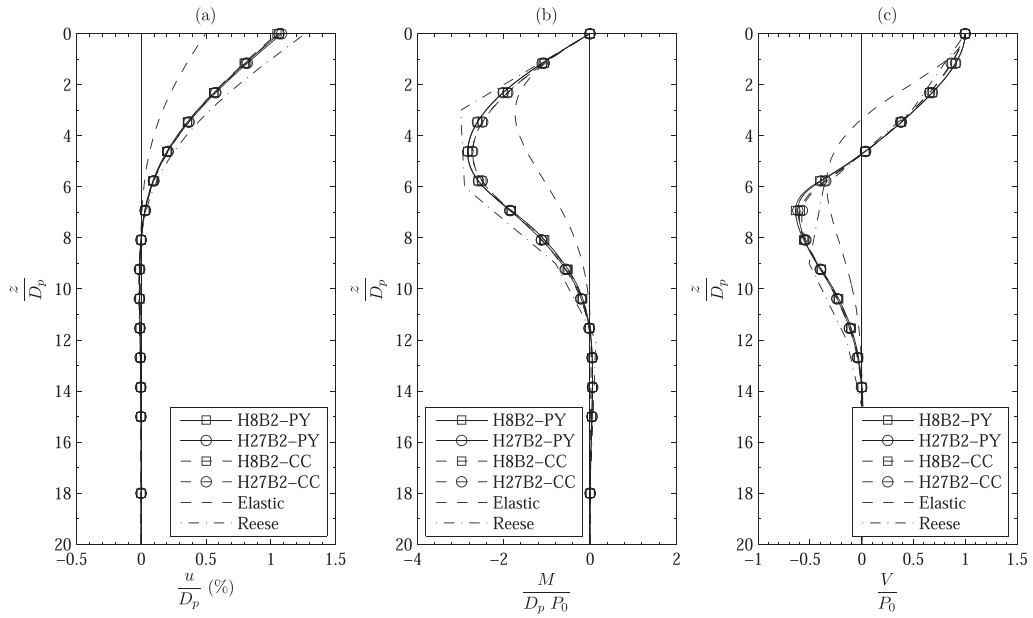

Figure 10. Pile in a cohesionless soil. Normalized results for H8B2 y H27B2 elements versus normalized depth: (a) lateral displacement u, (b) bending moment M y (c) shear force V.

Table II. Pile in a cohesionless soil. Normalized head displacements, distances and internal forces for the last load step.

EBE	$\frac{u_0}{D_p}(\%)$	$\frac{M_{max}}{D_p\,P_0}$	$\frac{z_{Mmax}}{D_p}$	$\frac{V_{max}}{P_0}$	$\frac{z_{Vmax}}{D_p}$
H8B2-PY	1.065	−2.835	4.615	−0.639	6.923
H27B2-PY	1.084	−2.829	4.615	−0.616	6.923
H8B2-CC	1.049	−2.722	4.712	−0.602	7.212
H27B2-CC	1.064	−2.715	4.712	−0.578	7.212

EBE, Embedded Beam Element.

elasto-plastic interfaces, for the last load step considered in the analysis.

Figure 11 shows curves of the lateral load P_0 versus the normalized head displacement u_0 obtained by means of the proposed formulation and the $p-y$ solution. The EBEs H8B2-PY and H27B2-PY (solid line in Figure 11) yield a slightly more flexible response than the EBEs H8B2-CC and H27B2-CC (dashed line in Figure 11). For low strains, the response obtained either by H8B2 or H27B2 elements, and both interfaces herein implemented, are tangent to the elastic response evaluated by means of the EBEs with perfect adherence between pile and soil (dashed line). For larger loads, the proposed EBE formulation with non-linear interface captures plastic strains. The global response, after the initial elastic range, is a little stiffer than the one obtained by means of the $p-y$ method (considering the Reese curves); however, the overall agreement is acceptable for engineering purposes. The H8B2-PY and H27B2-PY EBEs yields results closer to the ones obtained by means of the $p-y$ method.

It is noted that in the non-linear iterative Newton-Raphson scheme, the EBE's interfaces expressed in terms of solid kinematics show a better numerical behavior than the one obtained by means of the interface expressed in terms of beam kinematics.

5.3. Pipe pile in sand

This section describes the results obtained by means of the proposed formulation for a case study reported by Ashour *et al.* [11], consisting of a vertical pipe pile in sand. Figure 12 shows the basic features of the problem.

DOI: 10.1002/nag

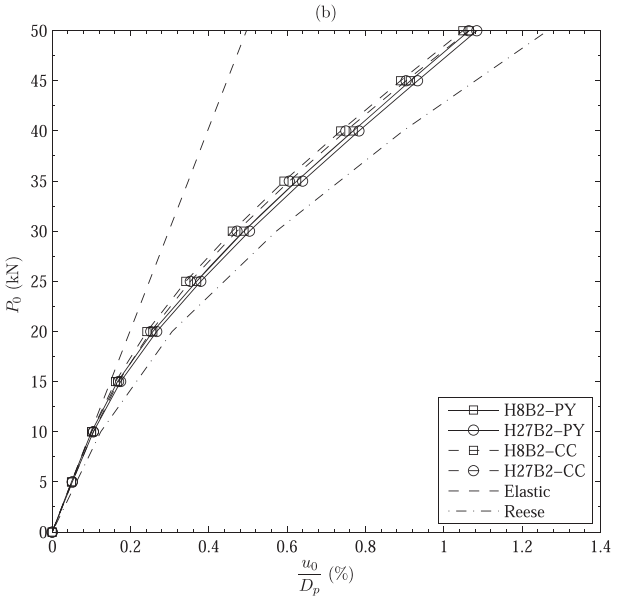

Figure 11. Pile in a cohesionless soil. Head external load P_0 versus normalized lateral displacements $\frac{u_0}{D_p}$.

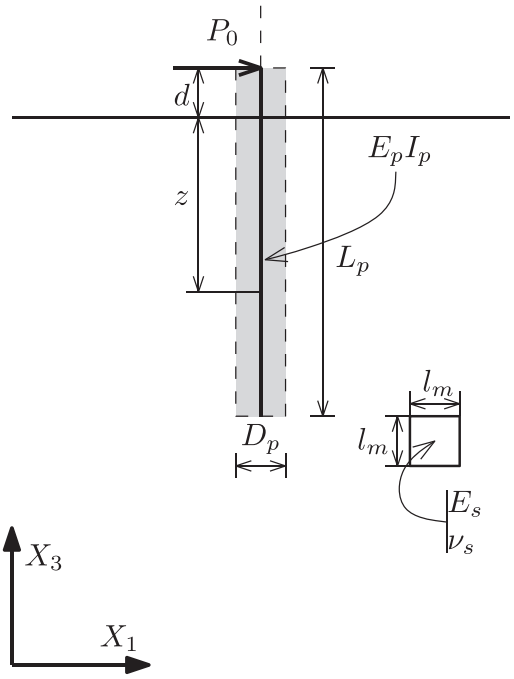

Figure 12. Pipe pile in sand. Lateral view of the three dimensional example.

The soil profile consists of a homogeneous submerged medium to dense sand [7] with the following parameters: Young's modulus $E_s = 100\,\text{MPa}$, Poisson coefficient $\nu_s = 0.25$, soil unit weight $\gamma_s = 18\,\text{kN/m}^3$, friction angle $\phi_s = 32°$.

The proposed non-linear interface, described in terms of beam kinematics, uses 1D-plasticity models with bi-linear hardening as shown in Figure 5-(a), for each component of $\mathbf{t'_d}$. These curves are characterized by means of the soil-pile lateral reaction modulus k_s, which is defined in terms of the soil and beam parameters, as proposed by Vesic [18]. The fictitious thickness of the interface $h_i = 0.10 D_p$, and the internal parameter a_y is adopted as $a_y = 0.20$.

DOI: 10.1002/nag

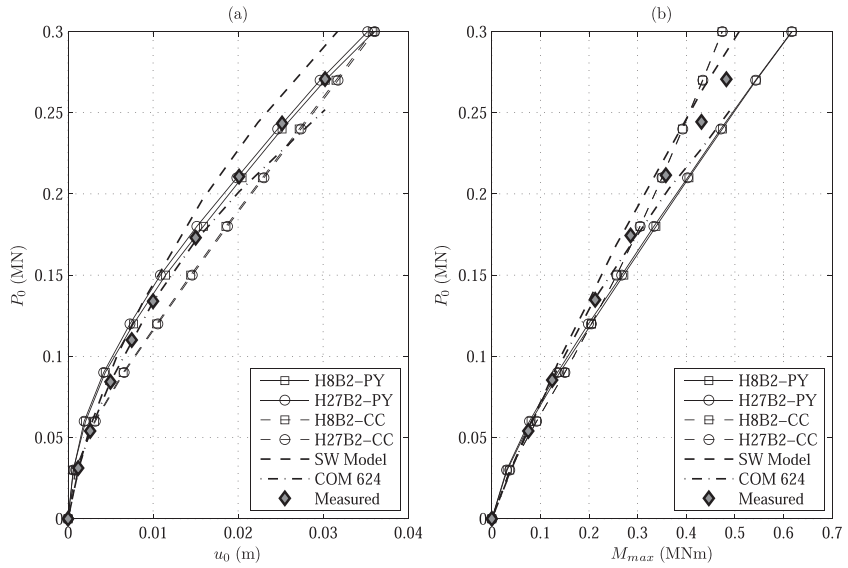

Figure 13. Pipe pile in sand. Results: (a) P_0 versus u_0 and (b) P_0 versus M_{max}.

The proposed interface described in terms of solid kinematics is based on a 3D elasto-plastic MCC model, whose parameters are as follows: internal material constant $\beta = 0.20$, tensile yield hydrostatic stress $p_t \approx 0\,\text{MPa}$, compressive yield hydrostatic stress $p_c = -\bar{\gamma}_s\, z$ ($\bar{\gamma}_s$ being the submerged unit weight of the soil), critical state line slope $M_c = \frac{6\sin(\phi_s)}{3-\sin(\phi_s)} = 1.287$, linear hardening modulus $H = 0.20$.

The pile parameters are as follows: bending stiffness $E_p I_p = 1.67 \times 10^5\,\text{kNm}^2$, length $L_p = 21.30\,\text{m}$, diameter $D_p = 0.61\,\text{m}$, cantilever length $d = 0.30\,\text{m}$ (Figure 12).

Figure 13-(a) shows the lateral displacements at the pile head, u_0, as a function of the applied lateral load, P_0. The numerical solution is in good agreement with the experimental observations obtained by the field load tests [7]. Figure 13-(a) also shows results obtained by means of the Strain Wedge (SW) method [11] and the computer program COM624 [22], which considers $p - y$ curves to represent the lateral soil response.

Figure 13-(b) displays the maximum bending moment, M_{max}, as a function of the applied lateral load, P_0, where it can be seen that there is good agreement between the proposed numerical solutions and the experimental results. It is observed that the proposed numerical solution obtained by means of the H8B2-CC and H27B2-CC EBEs yields more accurate results than the H8B2-PY and H27B2-PY EBEs. The latter ones agree better with the solution obtained by COM624 due to the fact that both methods are based on a very similar representation of the lateral soil reaction (i.e., $p - y$ curves).

As in the previous example, the numerical performance of the H8B2-CC and H27B2-CC EBEs in the iterative solution scheme is better than the H8B2-PY and H27B2-PY EBEs.

6. CONCLUSIONS

This paper presents the formulation of an elasto-plastic interface which, together with the EBE formulation presented in a previous paper by the authors, allows modeling laterally loaded piles considering the plasticity that develops in the near field, for the range of small-to-moderate displacements.

The interface introduces a relative displacement between solid and beam, referred to as a displacement jump, which represents the additional displacement with respect to elastic ground mass behavior because of plastic strains in the near field. The displacement jump can be described either in terms of beam or solid kinematics. These two alternatives require different constitutive model definitions in order to represent the non-linear soil behavior at the interface. The interface defined

DOI: 10.1002/nag

in terms of beam kinematics warrants a constitutive model that links distributed interaction a-forces and moments along the beam axis with displacement and rotation jumps associated with beam DOFs. In order to accomplish this, a 1D constitutive model, which is defined following $p-y$ curves widely used in engineering practice, is introduced for each displacement and rotation DOF. This interface has the advantage that this type of constitutive model is defined on the basis of experimental curves that are backed by an extensive database of load tests, performed on different types of soils and loading conditions. Thus, different $p-y$ (or $t-z$) curves can be introduced in a 3D framework for the coupled analysis of soil-structure interaction problems. As the $p-y$ method is defined in a single loading plane, a projection scheme is defined in order to account for the 3D nature of the problem. This procedure is implemented trough a projection operator $\mathcal{P}$, defined at every point of the beam axis.

As an alternative, an interface defined in terms of solid kinematics is presented, where the displacement jump is distributed along a thin domain, where plasticity can occur, representing the interaction surface ω. The fictitious thickness of this domain is an additional parameter of the model. In this case, the constitutive law can be introduced as a standard 3D plasticity model, which projected over the normal of the interaction surface yields the required non-linear interaction a-forces system. This interface concept has the advantage that the three-dimensionality of the problem is naturally accounted for. Moreover, many complex phenomena can be easily incorporated using this modeling approach; for example, pore pressure generation, installation effects, and gapping.

Both interface approaches have been implemented within the context of the FEM. The interface expressed in solid kinematics shows a better numerical behavior when using the Newton-Raphson non-linear iterative scheme. These interface models are particularly suitable for modeling problems where structural demands are due to free field ground deformations and the direction of the interaction force vector is not known beforehand; as for lateral spreading problems, ground movements due to nearby excavation or tunneling, as well as deformations due to surcharge loads applied in the ground near existing foundations.

Unlike the previous work of the authors [16], in the present formulation the soil-structure interaction problem cannot be exclusively written in terms of solid DOFs. Thus, the extra beam DOFs enlarge the size of the final equation system. However, all the other advantages inherent to the EBE-type formulations are preserved, including the fact that the pile location does not introduce restrictions to the mesh generation within the solid domain.

ACKNOWLEDGEMENTS

The authors acknowledge the partial financial support from UTN (Grant PID IN 1759), the support from SECyT UNC, and specially the PhD scholarship from CONICET, Argentina. P.J. Sánchez also acknowledges the financial support from the European Research Council under the FP7 (2007-2013) programme (ERC Grant agreement No. 320815 - Advanced Grant Project on Advanced tools for computational design of engineering materials COMP-DESMAT).

REFERENCES

1. Winkler E. *Die lehre von der elastizität und festigkeit (the theory of elasticity and stiffness)*, 1867. *H. Dominicus Prague, Czechoslovakia*.
2. Pasternak PL. *On a new method of analysis of an elastic foundation by means of two constants*, 1954. *Gosudarstvennoe Izdatelstvo Literaturi po Stroitelstvui Arkhitekture, Moscow, (in Russian)*.
3. Vlasov VZ, Leontiev UN. *Beams, plates and shells on elastic foundations*, 1966.
4. Bittnar Z, Šejnoha J. *Numerical Methods in Structural Engineering*. ASCE Press: New York, 1996.
5. Poulos HG. The behavior of laterally loaded piles i): single piles. *Journal of the Soil Mechanics and Foundations Division. ASCE* 1971; **97**(sm5):711–731.
6. Randolph MF. The response of flexible piles to lateral loading. *Geotechnique* 1981; **31**(2):247–259.
7. Reese LC, Cox WR, Koop FD. Analysis of laterally loaded piles in sand. *Proceedings, 5th Annual Offshore Technology Conference, Paper No. OTC 2080*, ASCE, Houston, Texas, 1974; 473–485.
8. Reese LC, Welch RC. Lateral loading of deep foundations in stiff clay. *Journal of the Geotechnical Engineering Division* 1975; **101**(7):633–649.
9. Norris GM. Theoretically based BEF laterally loaded pile analysis. In *3rd International Conference on Numerical Methods in Offshore Piling*. Inst Francais Du Petrole: Nantes, France, 1986; 361–386.

DOI: 10.1002/nag

10. Ashour M, Norris G, Pilling P. Lateral loading of a pile in layered soil using the strain wedge model. *Journal of Geotechnical and Geoenvironmental Engineering* 1998; **124**(4):303–315.
11. Ashour M, Norris G, Pilling P. Strain wedge model capability of analyzing behavior of laterally loaded isolated piles, drilled shafts, and pile groups. *Journal of Bridge Engineering* 2002; **7**(4):245–254.
12. Sadek M, Shahrour I. A three dimensional embedded beam element for reinforced geomaterials. *International Journal for Numerical and Analytical Methods in Geomechanics* 2004; **28**:931–946.
13. Engin HK, Septanika EG, Brinkgreve RBJ. Improved embedded beam elements for the modelling of piles. *Proceedings on 10th International Symposium on Numerical Models in Geotechnical Engineering–Numog X*, Rhodes (Greece), 2007.
14. Engin HK, Septanika EG, Brinkgreve RBJ. Estimation of pile group behavior using embedded piles. *The 12th International Conference of International Association for Computer Methods and Advances in Geomechanics (IACMAG)*, Goa, India, 2008; 1–6.
15. Engin HK, Septanika EG, Brinkgreve RBJ, Bonnier PG. Modelling piled foundations by means of embedded piles. *Proceedings of the 2nd International Workshop on Geotechnics of Soft Soils*, Glasgow, Scotland, 2008; 131–136.
16. Turello DF, Pinto F, Sánchez PJ. Embedded beam element with interaction surface for lateral loading of piles. *International Journal for Numerical and Analytical Methods in Geomechanics* 2016; **40**(4):568–582.
17. Simo JC, Hughes TJR. *Computational Inelasticity*. Springer-Verlag: New York, 2008.
18. Vesic AS. Beams on elastic subgrade and the Winkler's hypothesis. *fifth ICSMFE* 1961; **1**:845–850.
19. Neto EA, Periæ D, Owen DRJ. *Computational Methods for Plasticity: Theory and Applications*. John Wiley & Sons: The Atrium, Southern Gate, Chichester West Sussex PO19 8SQ, UK, 2008.
20. Bathe KJ. *Finite Element Procedures*. Klaus-Jurgen Bathe: Watertown, MA, 2006.
21. Reese LC, Cox WR, Koop FD. Analysis of laterally loaded piles in sand. *Proceedings. Sixth Annual Offshore Technology Conference*, 2080, Houston, Texas, 1974.
22. Reese LC, Sullivan WR. *Documentation of Computer Program Com 624: Parts I and II, Analysis of Stresses and Deflections for Laterally-Loaded Piles, Including Generation of PY Curves*. Geotechnical Engineering Software GS80-1, Geotechnical Engineering Center, Bureau of Engineering Research, University of Texas at Austin: Austin, Texas, 1980.

DOI: 10.1002/nag